



CrossMark  
click for updates

Cite this: *Chem. Sci.*, 2017, 8, 3270

## Quantifying the efficiency of CO<sub>2</sub> capture by Lewis pairs†

Jay J. Chi,<sup>a</sup> Timothy C. Johnstone,<sup>a</sup> Dan Voicu,<sup>a</sup> Paul Mehlmann,<sup>b</sup> Fabian Dielmann,<sup>b</sup> Eugenia Kumacheva<sup>\*a</sup> and Douglas W. Stephan<sup>\*a</sup>

A microfluidic strategy has been used for the time- and labour-efficient evaluation of the relative efficiency and thermodynamic parameters of CO<sub>2</sub> binding by three Lewis acid/base combinations, where efficiency is based on the amount of CO<sub>2</sub> taken up per binding unit in solution. Neither *t*Bu<sub>3</sub>P nor B(C<sub>6</sub>F<sub>5</sub>)<sub>3</sub> were independently effective at CO<sub>2</sub> capture, and the combination of the imidazolin-2-ylidenamino-substituted phosphine (Ni/Pr)<sub>3</sub>P and B(C<sub>6</sub>F<sub>5</sub>)<sub>3</sub> was equally ineffective. Nonetheless, an archetypal frustrated Lewis pair (FLP) comprised of *t*Bu<sub>3</sub>P and B(C<sub>6</sub>F<sub>5</sub>)<sub>3</sub> was shown to bind CO<sub>2</sub> more efficiently than either the FLP derived from tetramethylpiperidine (TMP) and B(C<sub>6</sub>F<sub>5</sub>)<sub>3</sub> or the highly basic phosphine (Ni/Pr)<sub>3</sub>P. Moreover, the proposed microfluidic platform was used to elucidate the thermodynamic parameters for these reactions.

Received 21st December 2016  
Accepted 17th February 2017

DOI: 10.1039/c6sc05607e

rsc.li/chemical-science

### Introduction

Anthropogenic carbon dioxide (CO<sub>2</sub>) emissions continue to climb to unprecedented levels and have played a key role in global climate change.<sup>1</sup> This worldwide issue has prompted many researchers to explore a wide variety of approaches to both reduce CO<sub>2</sub> emissions and lower CO<sub>2</sub> concentrations in the atmosphere. Efforts targeting the use of CO<sub>2</sub> as a C<sub>1</sub> chemical feedstock for conversion to formic acid, carbon monoxide,<sup>2</sup> or reusable fuels such as methane or methanol,<sup>3</sup> have prompted many studies targeting new catalyst development.<sup>4</sup> Although these developments offer the potential for disruptive technologies, it is important to note that the capture of CO<sub>2</sub> will be an integral component of any such advancement. A variety of approaches have been explored to capture CO<sub>2</sub> including the use of zeolites, silica gels, aluminas, and activated carbons,<sup>5</sup> as well as sophisticated metal-organic frameworks (MOFs).<sup>6</sup>

Investigations of the reactions of CO<sub>2</sub> with main group reagents have included a variety of amines,<sup>7</sup> alkanolamines<sup>8</sup> amidines, guanidines,<sup>9</sup> and *N*-heterocyclic carbenes (NHCs).<sup>10</sup> A decade ago, the use of frustrated Lewis pairs (FLPs) to capture CO<sub>2</sub> emerged with the report of Stephan, Erker, and coworkers who described intramolecular and intermolecular B/P-based FLPs for the capture of CO<sub>2</sub>.<sup>11</sup> Since then, a wide variety of B/N,<sup>12</sup> B/P,<sup>13</sup> Al/P,<sup>14</sup> and Si/P<sup>12a,15</sup> systems have been shown to capture or effect stoichiometric or catalytic reduction of CO<sub>2</sub>. In

a very recent development, Dielmann and coworkers described the synthesis of highly basic phosphines, generated by the inclusion of imidazolin-2-ylidenamino substituents.<sup>16</sup> These are the first phosphines to be shown to sequester CO<sub>2</sub> in the absence of the Lewis acid necessary to form an FLP.<sup>17</sup>

Although a number of FLP and main group systems have been shown to capture CO<sub>2</sub>,<sup>13c</sup> the ability to quantitatively compare the efficiency of such systems remains experimentally challenging. Standard batch-scale characterization methods for reactions at the CO<sub>2</sub> gas-liquid interface suffer from long reaction times and are often diffusion controlled.<sup>18</sup> Recently, Kumacheva and coworkers developed a microfluidic (MF) platform for the study of gas/liquid reactions.<sup>19</sup> The MF methodology was validated for the well-studied CO<sub>2</sub> reaction with amine<sup>19b</sup> and used small amounts of reagents thus providing fast and cost-efficient access to thermodynamic data for gas/liquid reactions (10–15 min per experiment).



Fig. 1 (a) Schematic depiction of the MF gas/liquid device. (b) Magnified view of the outlined region shown in (a), which shows the shrinkage of the gas plugs as they flow through the channel.

<sup>a</sup>Department of Chemistry, University of Toronto, 80 St. George St., Toronto, Ontario M5S 3H6, Canada. E-mail: dstephan@chem.utoronto.ca

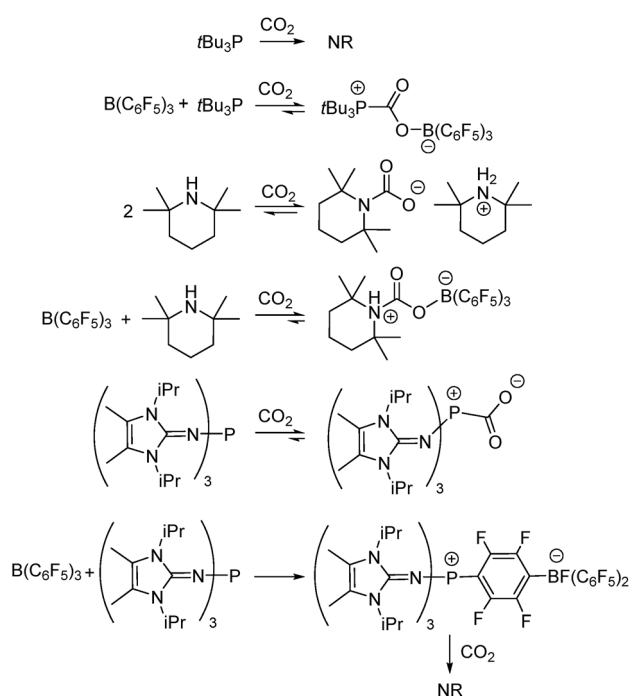
<sup>b</sup>Institut für Anorganische und Analytische Chemie, Westfälische Wilhelms-Universität Münster, Corrensstrasse 30, 48149 Münster, Germany

† Electronic supplementary information (ESI) available. See DOI: 10.1039/c6sc05607e



In Fig. 1, a gas and a reagent solution are supplied to two inlets of a MF reactor. At a Y-junction, the gaseous stream breaks up in a periodic manner to generate uniformly sized gas plugs that are separated by liquid segments (slugs). As alternating gas plugs and solution slugs flow through the MF channel, the dissolution of the gas and its reaction with reagents in the solution results in a decrease in the volume of gas plugs with time (or the distance from the Y-junction). Analysis of digitized images of the gas plugs allows for the quantification of gas consumption using the ideal gas law.<sup>19a,20</sup> After a particular time (directly related to distance in the MF reactor), the dissolved reagents and the gas reach equilibrium, and the gaseous plug volume remains constant. This enables the determination of the equilibrium constant of the reaction, and a study of the reaction at different temperatures enables assessment of the thermodynamic parameters,  $\Delta G^\circ$ ,  $\Delta H^\circ$ , and  $\Delta S^\circ$ . The validity of this methodology was demonstrated with the study of the sequestration of CO<sub>2</sub> by the FLP, ClB(C<sub>6</sub>F<sub>5</sub>)<sub>2</sub>/tBu<sub>3</sub>P.<sup>19a,20</sup>

In the present work, this innovative MF approach has been applied to compare the efficiency of CO<sub>2</sub> sequestration in reactions of three Lewis acid–base combinations with CO<sub>2</sub>. The prototypical FLP tBu<sub>3</sub>P/B(C<sub>6</sub>F<sub>5</sub>)<sub>3</sub>, as well as the FLP derived from tetramethylpiperidine (TMP)/B(C<sub>6</sub>F<sub>5</sub>)<sub>3</sub>, were investigated. In addition, the extremely basic imidazolin-2-ylidenamino-substituted phosphine (NIiPr)<sub>3</sub>P was investigated alone and in combination with B(C<sub>6</sub>F<sub>5</sub>)<sub>3</sub>. Although each of these systems is known to bind CO<sub>2</sub> (Scheme 1),<sup>11,12b,17b</sup> the present MF study provides qualitative and quantitative comparisons of this CO<sub>2</sub> binding. Such data afford insights that are important for the design of main group systems for CO<sub>2</sub> capture.



Scheme 1 Reactions of Lewis acid–base combinations with CO<sub>2</sub>. NR = no reaction.

## Results and discussion

The established MF protocol<sup>19a</sup> was used to determine the thermodynamic parameters associated with the reaction of CO<sub>2</sub> with combinations of the Lewis acid B(C<sub>6</sub>F<sub>5</sub>)<sub>3</sub> and one of the Lewis bases, tBu<sub>3</sub>P, TMP, or (NIiPr)<sub>3</sub>P. Bromobenzene was selected as a suitable solvent due to its low volatility and the solubility of the reagents and corresponding CO<sub>2</sub> adducts. In an initial reference experiment, physical dissolution of CO<sub>2</sub> gas in bromobenzene was characterized by the temporal variation in the concentration of physically dissolved CO<sub>2</sub> (*i.e.*, [CO<sub>2</sub>]<sub>dissolved</sub>) by analysing the digitized dimensions of alternating slugs of solvent and plugs of CO<sub>2</sub> flowing through the MF reactor. By monitoring the decrease in CO<sub>2</sub> plug volume and applying the ideal gas law<sup>19a</sup> (eqn (1) and (2), see ESI, Fig. S1 and S2†), the number of moles of CO<sub>2</sub> transferred from the gas plug to the adjacent liquid slug at time *t*, *n*<sub>CO<sub>2</sub></sub>(*t*), was determined. The equilibrium concentration of physically dissolved CO<sub>2</sub> (*C*<sub>tot</sub>) was reached after approximately 2 s (Fig. 2).

$$n_{\text{CO}_2}(t) = \frac{PV_p(t)}{RT} \quad (1)$$

$$C_{\text{tot}}(t) = \frac{n_{\text{CO}_2}(t=0) - n_{\text{CO}_2}(t)}{V_s(t)} \quad (2)$$

*n*<sub>CO<sub>2</sub></sub>(*t*): moles of CO<sub>2</sub> in the plug at time *t*; *P*: pressure; *V*<sub>p</sub>(*t*): volume of CO<sub>2</sub> at time *t*, *R*: gas constant (8.314 J mol<sup>-1</sup> K<sup>-1</sup>); *T*: temperature; *V*<sub>s</sub>(*t*): volume of the liquid solution at time *t*.

The addition of either B(C<sub>6</sub>F<sub>5</sub>)<sub>3</sub>, or tBu<sub>3</sub>P independently to the solvent had little effect on the equilibrium concentration of CO<sub>2</sub> in the liquid slugs, beyond the dissolution of CO<sub>2</sub> in bromobenzene (Fig. 2a). However, combining B(C<sub>6</sub>F<sub>5</sub>)<sub>3</sub> and tBu<sub>3</sub>P in solution resulted in increased CO<sub>2</sub> uptake, which further increased with elevated FLP concentration. These observations are consistent with the known inability of the individual components to capture CO<sub>2</sub>, and the established efficacy with which CO<sub>2</sub> is captured by this FLP. These observations are also consistent with our earlier MF study of CO<sub>2</sub> capture by the related ClB(C<sub>6</sub>F<sub>5</sub>)<sub>2</sub>/tBu<sub>3</sub>P FLP.<sup>19a</sup>

Investigation of the FLP derived from B(C<sub>6</sub>F<sub>5</sub>)<sub>3</sub> and TMP revealed that TMP alone in solution is able to sequester CO<sub>2</sub> (Fig. 2b, ■), consistent with the known ability of secondary amines to reversibly bind CO<sub>2</sub>.<sup>12b</sup> It is noteworthy, however, that the concurrent presence of B(C<sub>6</sub>F<sub>5</sub>)<sub>3</sub> in solution results in a significantly enhanced CO<sub>2</sub> uptake. Again, increasing concentration of the FLP results in increased CO<sub>2</sub> sequestration.

In sharp contrast to tBu<sub>3</sub>P, increasing concentrations of (NIiPr)<sub>3</sub>P led to increasing capture of CO<sub>2</sub> (Fig. 3). These observations are consistent with the work of Dielmann and coworkers<sup>17b</sup> who have demonstrated the ability of imidazolin-2-ylidenamino-substituted phosphines to bind CO<sub>2</sub>. In further contrast, addition of B(C<sub>6</sub>F<sub>5</sub>)<sub>3</sub> to solutions of (NIiPr)<sub>3</sub>P inhibited CO<sub>2</sub> uptake beyond the physical dissolution of CO<sub>2</sub> into the solvent (■ vs. ◆, Fig. 2c). This result indicates an irreversible reaction of (NIiPr)<sub>3</sub>P with B(C<sub>6</sub>F<sub>5</sub>)<sub>3</sub>. Monitoring of this reaction by NMR spectroscopy supports the formation of several





Fig. 2 Variation in total concentration of CO<sub>2</sub> transferred at 293 K from gas plugs to reagent solution slugs plotted as a function of time. The gaps in the data from 1.5 s to 2.0 s result from the exclusion of microchannel bends outside the region of interest (see ESI, Fig. S1†). (a) Plots for the FLP derived from *t*Bu<sub>3</sub>P and B(C<sub>6</sub>F<sub>5</sub>)<sub>3</sub>. (b) Plots for the FLP derived from TMP and B(C<sub>6</sub>F<sub>5</sub>)<sub>3</sub>. (c) Plots for the combination of (Ni/Pr)<sub>3</sub>P and B(C<sub>6</sub>F<sub>5</sub>)<sub>3</sub>. For C<sub>6</sub>H<sub>5</sub>Br alone (◆), C<sub>tot</sub> = [CO<sub>2</sub>]<sub>dissolved</sub>. Each experimental point represents the average of three experiments conducted under identical conditions, where 300 images were acquired for each experiments with a minimum of 4000 CO<sub>2</sub> plugs.

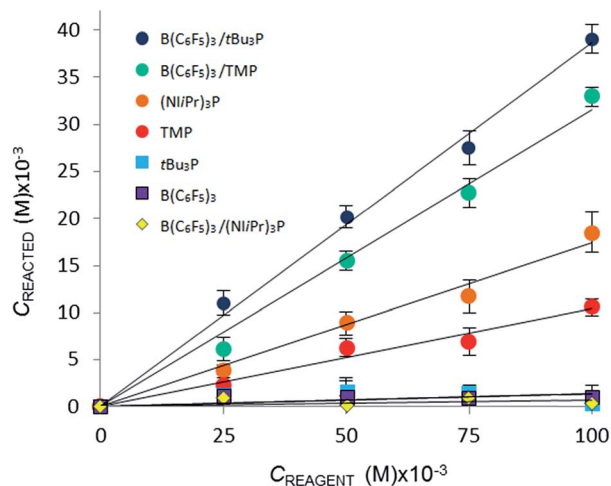


Fig. 3 Variation in equilibrium concentration of CO<sub>2</sub> ( $C_{\text{reacted}}$ ) plotted as a function of initial reagent concentration at  $T = 293$  K (repeated in triplicate, analysing 300 images with a range of 4000–7000 plugs of CO<sub>2</sub>).

products, including the zwitterionic product (Ni/Pr)<sub>3</sub>PC<sub>6</sub>F<sub>4</sub><sup>-</sup>BF(C<sub>6</sub>F<sub>5</sub>)<sub>2</sub> as the major species (Scheme 1, see ESI†). Analogous products have been previously reported for sterically encumbered, basic phosphines.<sup>21</sup> Presumably, the highly basic nature of the phosphine (Ni/Pr)<sub>3</sub>P prompts this reactivity with B(C<sub>6</sub>F<sub>5</sub>)<sub>3</sub> and precludes capture of CO<sub>2</sub>.

The CO<sub>2</sub> uptake caused directly by chemical reaction,  $C_{\text{reacted}}$ , was determined by subtracting the [CO<sub>2</sub>]<sub>dissolved</sub> (for the CO<sub>2</sub>-bromobenzene system) from the total equilibrium uptake of CO<sub>2</sub>,  $C_{\text{tot}}$ , for each reagent. A plot of  $C_{\text{reacted}}$  against reagent concentration illustrates the relative efficacy of the reaction of CO<sub>2</sub> with the Lewis acid, Lewis base, or Lewis acid–base combination (Fig. 3).

Using the concentration data allows determination of the equilibrium constants ( $K_{\text{eq}}$ ) for each system. In eqn (3), [CO<sub>2</sub> adduct] is equal to  $C_{\text{reacted}}$  (determined from Fig. 3), the [Lewis acid] and [Lewis base] are calculated directly by subtracting  $C_{\text{reacted}}$  from the initial reagent concentrations, and [CO<sub>2</sub>]<sub>dissolved</sub> is the equilibrium concentration of CO<sub>2</sub> dissolved in bromobenzene (Fig. 2). In this fashion, the room temperature equilibrium constants for CO<sub>2</sub> binding for *t*Bu<sub>3</sub>P/B(C<sub>6</sub>F<sub>5</sub>)<sub>3</sub>, TMP/B(C<sub>6</sub>F<sub>5</sub>)<sub>3</sub>, and (Ni/Pr)<sub>3</sub>P were determined and are collected in Table 1. The data shown in Fig. 3 reveal that the FLP systems derived from *t*Bu<sub>3</sub>P or TMP with B(C<sub>6</sub>F<sub>5</sub>)<sub>3</sub> are more efficient at CO<sub>2</sub> capture by 29% and 16%, respectively, than the highly basic phosphine, (Ni/Pr)<sub>3</sub>P. In this context, efficiency is taken to be the amount of CO<sub>2</sub>, per binding unit, sequestered by the binding reagents. These data also illustrate that the FLP *t*Bu<sub>3</sub>P/B(C<sub>6</sub>F<sub>5</sub>)<sub>3</sub> is 11% more efficient at CO<sub>2</sub> uptake than the FLP derived from TMP/B(C<sub>6</sub>F<sub>5</sub>)<sub>3</sub>. Thus, although previously reported NMR experiments demonstrated the ability of these systems to bind CO<sub>2</sub>, the present MF methodology provides a fast, efficient and high-throughput platform for quantitative ranking of the ability of these systems to bind CO<sub>2</sub> at ambient temperature.



Table 1 Thermodynamic parameters for CO<sub>2</sub> capture determined by the MF method<sup>a</sup>

Reagents	$K_{\text{eq}}$ (293 K)	$\Delta H_{293}^b$ kJ mol <sup>-1</sup>	$\Delta S_{293}$ J mol <sup>-1</sup> K <sup>-1</sup>	$\Delta G_{293}$ kJ mol <sup>-1</sup>
<i>t</i> Bu <sub>3</sub> P/B(C <sub>6</sub> F <sub>5</sub> ) <sub>2</sub> Cl <sup>19a</sup>	223 M <sup>-2</sup>	-39.3	-89.3	-14.8
<i>t</i> Bu <sub>3</sub> P/B(C <sub>6</sub> F <sub>5</sub> ) <sub>3</sub>	517 M <sup>-2</sup>	-100.0	-289.3	-15.2
TMP/B(C <sub>6</sub> F <sub>5</sub> ) <sub>3</sub>	267 M <sup>-2</sup>	-73.8	-205.4	-13.6
(Ni <sup>i</sup> Pr) <sub>3</sub> P	4158 M <sup>-1</sup>	-29.1	-30.8	-20.0

<sup>a</sup> Additional values for 273 K, 283 K, 303 K, and 313 K are deposited in the ESI (Table S2–S4). <sup>b</sup> The value for  $\Delta H$  is determined by the corresponding slope in Fig. 5.

The reactions of *t*Bu<sub>3</sub>P/B(C<sub>6</sub>F<sub>5</sub>)<sub>3</sub>, TMP/B(C<sub>6</sub>F<sub>5</sub>)<sub>3</sub>, and (Ni<sup>i</sup>Pr)<sub>3</sub>P with CO<sub>2</sub> were also studied in the temperature range from 273 to 313 K. A plot of the amount of CO<sub>2</sub> captured ( $C_{\text{reacted}}$ ) versus the concentration of either the FLPs or (Ni<sup>i</sup>Pr)<sub>3</sub>P was monotonic and linear. Due to the exothermic nature of the reactions,<sup>19a,20</sup> as the reaction systems were cooled, the degree of CO<sub>2</sub> capture was enhanced at each of the concentrations of reagents (Fig. 4). Using the values of  $K_{\text{eq}}$  at different temperatures, the corresponding Gibbs free energy for each reaction can be obtained (eqn (4)). The use of a van't Hoff plot (Fig. 5; eqn (5)) allows the determination of the corresponding enthalpy ( $\Delta H^\circ$ ) and entropy ( $\Delta S^\circ$ ) values (Table 1). The linearity of the association between  $\ln(K_{\text{eq}})$  and  $1/T$  indicates that enthalpy does not change appreciably within the temperature range investigated. It is noted that the  $\Delta H^\circ$  of the reaction of B(C<sub>6</sub>F<sub>5</sub>)<sub>3</sub>, *t*Bu<sub>3</sub>P, and CO<sub>2</sub>, -100.0 kJ mol<sup>-1</sup>, is in excellent agreement with the value of -100.4 kJ mol<sup>-1</sup> obtained calorimetrically by Autrey and coworkers.<sup>22</sup>

$$K_{\text{eq}} = \frac{[\text{CO}_2 \text{ adduct}]}{[\text{Lewis acid}][\text{Lewis base}][\text{CO}_2]_{\text{dissolved}}} \quad (3)$$

$$\Delta G^\circ = -RT \ln(K_{\text{eq}}) \quad (4)$$

$$\ln(K_{\text{eq}}) = -\frac{\Delta H^\circ}{RT} + \frac{\Delta S^\circ}{R} \quad (5)$$



Fig. 4 Variation in the equilibrium concentration of captured CO<sub>2</sub>, plotted as a function of initial FLP (B(C<sub>6</sub>F<sub>5</sub>)<sub>3</sub> and *t*Bu<sub>3</sub>P) concentration at  $T = 273$  K, 283 K, 293 K, 303 K, and 313 K (repeated in triplicate analysing 300 images with a range of 4000–7000 plugs of CO<sub>2</sub>) (see ESI† for plots for the other systems).

To gain further insight, theoretical calculations were performed using Density Functional Theory (DFT) at the M11/6-311G(d,p) level of theory.<sup>23</sup> The optimized geometries of B(C<sub>6</sub>F<sub>5</sub>)<sub>3</sub>, *t*Bu<sub>3</sub>P, CO<sub>2</sub>, and *t*Bu<sub>3</sub>PCO<sub>2</sub>B(C<sub>6</sub>F<sub>5</sub>)<sub>3</sub> were computed using the integral equation formalism variant of the polarizable continuum model (IEFPCM) to implicitly assess the effects of solvation by bromobenzene.<sup>24</sup> Frequency calculations confirmed that each structure was at a minimum on its potential energy surface and provided partition functions from which thermodynamic parameters were computed. The reaction enthalpy obtained at this level of theory, -176 kJ mol<sup>-1</sup>, was significantly larger than the experimental value of -100.0 kJ mol<sup>-1</sup>. To further investigate this discrepancy, the calculations were carried out at the B2PLYP-D3/6-311G(d,p) level of theory.<sup>25</sup> This double hybrid meta-GGA method includes an empirical long-range dispersion correction and performs well in the evaluation of main group thermochemistry.<sup>26</sup> A recent study comparing the ability of M11 and B2PLYP-D3 to evaluate the chemistry of compounds for which dispersive interactions are important found the latter to consistently outperformed the former.<sup>27</sup> The internal reaction energy for CO<sub>2</sub> capture by the B(C<sub>6</sub>F<sub>5</sub>)<sub>3</sub>/*t*Bu<sub>3</sub>P FLP was computed to be -129 kJ mol<sup>-1</sup> at this double hybrid level of theory. This value more closely approaches the experimental reaction enthalpy. In addition, if this internal reaction energy is used in combination with the reaction entropy obtained at the M11/6-311G(d,p) level of theory, then the Gibbs free energy of the reaction computed at ambient temperature is -15.4 kJ mol<sup>-1</sup>, in excellent agreement with the experimental value of -15.2 kJ mol<sup>-1</sup>.<sup>28</sup>



Fig. 5 Plot of  $\ln(K_{\text{eq}})$  vs.  $1/T$  ( $T$  ranging from 273 K to 313 K).







- 12 (a) A. E. Ashley, A. L. Thompson and D. O'Hare, *Angew. Chem., Int. Ed.*, 2009, **48**, 9839; (b) A. Berkefeld, W. E. Piers and M. Parvez, *J. Am. Chem. Soc.*, 2010, **132**, 10660–10661.
- 13 (a) R. Declercq, G. Bouhadir, D. Bourissou, M.-A. Légaré, M.-A. Courtemanche, K. S. Nahi, N. Bouchard, F.-G. Fontaine and L. Maron, *ACS Catal.*, 2015, **5**, 2513–2520; (b) M.-A. Courtemanche, M.-A. Légaré, L. Maron and F.-G. Fontaine, *J. Am. Chem. Soc.*, 2014, **136**, 10708–10717; (c) T. Wang and D. W. Stephan, *Chem. Commun.*, 2014, **50**, 7007–7010.
- 14 (a) M.-A. Courtemanche, J. Larouche, M.-A. Légaré, W. Bi, L. Maron and F.-G. Fontaine, *Organometallics*, 2013, **32**, 6804–6811; (b) G. Ménard and D. W. Stephan, *J. Am. Chem. Soc.*, 2010, **132**, 1796–1797; (c) G. Ménard and D. W. Stephan, *Angew. Chem., Int. Ed.*, 2011, **50**, 8396–8399.
- 15 (a) S. A. Weicker and D. W. Stephan, *Chem.–Eur. J.*, 2015, **21**, 13027–13034; (b) M. Reißmann, A. Schäfer, S. Jung and T. Müller, *Organometallics*, 2013, **32**, 6736–6744.
- 16 M. A. Wünsche, P. Mehlmann, T. Witteler, F. Buß, P. Rathmann and F. Dielmann, *Angew. Chem., Int. Ed.*, 2015, **54**, 11857–11860.
- 17 (a) F. Buß, P. Mehlmann, C. Mück-Lichtenfeld, K. Bergander and F. Dielmann, *J. Am. Chem. Soc.*, 2016, **138**, 1840–1843; (b) P. Mehlmann, C. Mück-Lichtenfeld, T. T. Y. Tan and F. Dielmann, *Chem.–Eur. J.*, DOI: 10.1002/chem.201604971.
- 18 S. Bishnoi and G. T. Rochelle, *Chem. Eng. Sci.*, 2000, **55**, 5531–5543.
- 19 (a) D. Voicu, M. Abolhasani, R. Choueiri, G. Lestari, C. Seiler, G. Menard, J. Greener, A. Guenther, D. W. Stephan and E. Kumacheva, *J. Am. Chem. Soc.*, 2014, **136**, 3875–3880; (b) W. Li, K. Liu, R. Simms, J. Greener, D. Jagadeesan, S. Pinto, A. Gunther and E. Kumacheva, *J. Am. Chem. Soc.*, 2012, **134**, 3127–3132.
- 20 D. Voicu, D. W. Stephan and E. Kumacheva, *ChemSusChem*, 2015, **8**, 4202–4208.
- 21 (a) G. C. Welch, R. R. San Juan, J. D. Masuda and D. W. Stephan, *Science*, 2006, **314**, 1124–1126; (b) G. C. Welch, L. Cabrera, P. A. Chase, E. Hollink, J. D. Masuda, P. R. Wei and D. W. Stephan, *Dalton Trans.*, 2007, 3407–3414.
- 22 A. Karkamkar, K. Parab, D. M. Camaioni, D. Neiner, H. Cho, T. K. Nielsen and T. Autrey, *Dalton Trans.*, 2013, **42**, 615–619.
- 23 (a) R. Krishnan, J. S. Binkley, R. Seeger and J. A. Pople, *J. Chem. Phys.*, 1980, **72**, 650–654; (b) R. Peverati and D. G. Truhlar, *J. Phys. Chem. Lett.*, 2011, **2**, 2810–2817; (c) A. D. McLean and G. S. Chandler, *J. Chem. Phys.*, 1980, **72**, 5639–5648.
- 24 J. Tomasi, B. Mennucci and R. Cammi, *Chem. Rev.*, 2005, **105**, 2999–3094.
- 25 (a) S. Grimme, *J. Chem. Phys.*, 2006, **124**, 034108–034116; (b) S. Grimme, S. Ehrlich and L. Goerigk, *J. Comput. Chem.*, 2011, **32**, 1456–1465.
- 26 L. Goerigk and S. Grimme, *J. Chem. Theory Comput.*, 2011, **7**, 291–309.
- 27 L. Goerigk, *J. Phys. Chem. Lett.*, 2015, **6**, 3891–3896.
- 28 Computed thermochemical parameters for the binding of CO<sub>2</sub> by (NiPr)<sub>3</sub>P afforded values significantly greater than those reported here (ref. 17b). Preliminary follow-up computations suggest that a monotonic relationship between the amount of Hartree–Fock exchange included and the computed internal energy of reaction for CO<sub>2</sub> binding to (NiPr)<sub>3</sub>P. While we do not as of yet have an explanation for this observation, it is noted that the present computations show better agree with the experimental values derived herein.

